Volume 17, Number 1, 2024. pp. 59-73

Jordan Journal of Physics

ARTICLE

Influence of Ar:O_2 Mixing Ratio on Characteristics of Tio$_2$ Nanostructured Thin Films Deposited by DC Reactive Magnetron Sputtering Method

Adnan Mini[a], **M. B. Karman**[b] and **Rahaf Daoun**[a]

[a] *Department of Physics, Faculty of Science, Tishreen University.*
[b] *Department of Physics, Faculty of Science, Aleppo University.*

Doi: **https://doi.org/10.47011/17.1.6**

Received on: 29/04/2022; Accepted on: 30/06/2022

Abstract: In this paper, titanium dioxide nanostructured thin films TiO_2 were deposited on unheated glass substrates by applying the DC reactive magnetron sputtering method. Three TiO_2 films were deposited using argon sputtering gas with different oxygen ratios: 10%, 25%, and 50%. The resulting films had thicknesses of 200, 184, and 140 nm, respectively. The structural, morphological, optical, and electrical properties of deposited thin films were studied. X-ray diffraction (XRD) data showed that the samples exhibited an amorphous phase. It was found from atomic force microscopy (AFM) that the deposited thin films had a nanostructure, and the heights of their nanograins were 16, 24, and 30 nm, respectively. It was observed from the root-mean-square height RMS values that the films had low roughness. The UV-Vis-NIR spectroscopy showed that the films become more transparent with the increase in oxygen content. The direct band gap ranged between 3.68 and 3.88 eV, while the indirect band gap ranged from 3.3 to 3.66 eV. The highest intensity photoluminescence emission was obtained for the film deposited at 50% O_2. In addition, the impedance spectroscopy showed that the films' resistance did not change with changing oxygen content.

Keywords: Magnetron sputtering, Titanium dioxide, X-ray diffraction, Absorption spectra, Atomic Force Microscopy, Photoluminescence, Impedance.

1. Introduction

In recent years, thin films of titanium dioxide (TiO_2) have been extensively studied, due to their features and properties that serve a wide range of applications. Originally employed as a pigment in paints, coatings, and sunscreen since their commercial production in the 20th century, it has found expanded utility in diverse fields such as solar cells [3], gas sensors [4, 5], photocatalysts [1, 6], and more. Titanium dioxide (TiO_2) is an n-type semiconductor with a wide energy band gap [7]. A thin film of TiO_2 offers attractive features, due to its high refractive index [8], good chemical stability [9], and transparency in the visible and near-infrared regions [10]. TiO_2 thin film crystallizes in three phases: rutile, anatase, and brookite, in addition to the amorphous phase [11]. TiO_2 thin films can be deposited by various methods, such as pulsed laser deposition (PLD) [12, 13], chemical bath deposition (CBD) [14], spin-coating [15], electron beam evaporation [16], and direct current (DC) or radio frequency (RF) magnetron sputtering [8, 17]. DC reactive magnetron sputtering technique provides homogeneous, pure, and dense TiO_2 thin films on large area substrates at low temperatures [18, 19]. The structural, morphological, and optical properties of thin films can be affected by changing

Corresponding Author: Rahaf Daoun **Email**: daounr93@gmail.com

deposition parameters, such as reactive gas ratio [18], deposition power [9], substrate type [20, 21], distance between target and substrate [22], deposition temperature [8], etc. This study focuses on the effect of oxygen ratio on the structural, morphological, optical, and electrical properties of nanostructured TiO_2 thin films synthesized by DC reactive magnetron sputtering.

2. Experimental Details

2.1 Materials and Deposition Method:

Thin films of titanium dioxide TiO_2 were deposited on glass substrates by the HHV Lab Coater Auto 500 magnetron sputtering system. This system consists of a stainless-steel sputtering chamber with a mechanical pump and a diffusion pump. The sputtering chamber contains two electrodes (anode and cathode) that are connected to a DC power supply to generate plasma. To carry out the deposition process, a pure titanium target (99.9% purity) with a 76.2 mm diameter was used. The substrates have been cleaned with ethanol and deionized water, then dried thoroughly. The deposition parameters were entered via a digital control panel. The deposition process was carried out in an atmosphere of argon, using oxygen as reactive gas at the ratios of 10%, 25%, and 50%. A pre-sputtering of the target surface was performed before the reactive gas was entered. Deposition parameters are tabulated in Table 1.

TABLE 1. Deposition parameters.

Parameter	Value
Target-substrate distance $D_{s\text{-}t}$	13cm
Base pressure	5×10^{-6} mbar
Sputtering power P	550W
Voltage V	700-800V
Current I	1000mA
Deposition pressure	0.117-0.141 mbar
Deposition time D_t	20 min

2.2 Thickness d and Deposition Rate DR:

Film thicknesses d were determined by the optical method. Deposition rate D_R of TiO_2 thin films was calculated by relation [23]:

$$D_R = \frac{d}{D_t} \tag{1}$$

Values of thicknesses and deposition rates of TiO_2 thin films are listed in Table 2.

TABLE 2. Height and feature parameters of TiO_2 thin films according to ISO-25178-Roughness.

O_2 %	10	25	50
d(nm) Thickness	200	184	140
D_R (nm/min)	10	9.2	7
Height parameters			
Sq (nm) root-mean-square height	1.796	2.464	1.446
Sa (nm) arithmetic mean height	1.300	1.655	0.6329
Ssk skewness	1.142	1.902	3.489
Sku kurtosis	17.85	21.35	120.7
Feature parameters			
Spd (1/µm^2) density of peaks	7.367	9.671	0.3748
Spc (1/µm) arithmetic mean peak curvature	3.426	3.789	5.614

2.3 Characterization Techniques:

1. Structural properties: The structural properties of TiO_2 thin films were examined by X-ray diffraction (XRD) technique (Leybold Didactic 554-81), using Cu Kα (λ = 1.5405 A°) radiation, 35KV-1mA. Diffractograms were obtained by scanning from 20° to 80° at 2θ steps of 0.1° and a scan step time of 10 s.
2. Surface morphology: Surface morphology was examined using atomic force microscopy (AFM) (Nanosurf Naio AFM-HALCYONIC). Height parameters and feature parameters were studied by using the Mountains Lab program according to ISO-25178, by applying a Gaussian filter (with 0.25 µm cutoff wavelength).

3. Optical properties: The optical transmittance of the films was measured by UV-Vis-NIR spectrophotometer (Jasco V-670) in the wavelength range of 300-2000 nm.
4. Photoluminescence properties: The fluorescence spectra of as-deposited films were measured using a fluorescence spectrometer FS-2/SCINCO. Emission and excitation measurements were performed in the wavelength range of 200-900 nm. An electron excitation energy greater than the band gap of the films was applied.
5. Impedance spectroscopy: To plot the complex impedance spectrum, a gain phase analyzer (Schlumberger-SI 1253) was used. This device was used in the range of frequencies (0.1Hz- 20KHz).

3. Results and Discussions

3.1 Structural Properties:

Fig. 1 shows the XRD patterns of the TiO_2 thin films as deposited onto glass at different oxygen ratios. It was noted that all the films have an amorphous phase. According to Serio *et al.* [24], there are two main factors to film crystallization during the deposition process: the thermal energy provided by heating the substrate and the energy of the particles that are deposited on the substrate. In our study, the amorphous structure of the films can be attributed to amorphous substrates, low deposition power, the large distance between the target and substrate, and the deposition without heating the samples. This result agrees with Sekhar *et al.* who attributed the amorphous phase to the low surface mobility of deposited particles [25]. Shen *et al.* [26] and Rabih *et al.* [23] attribute the amorphous nature of TiO_2 thin films to the fact that the low energy of deposition particles was not enough for crystallization.

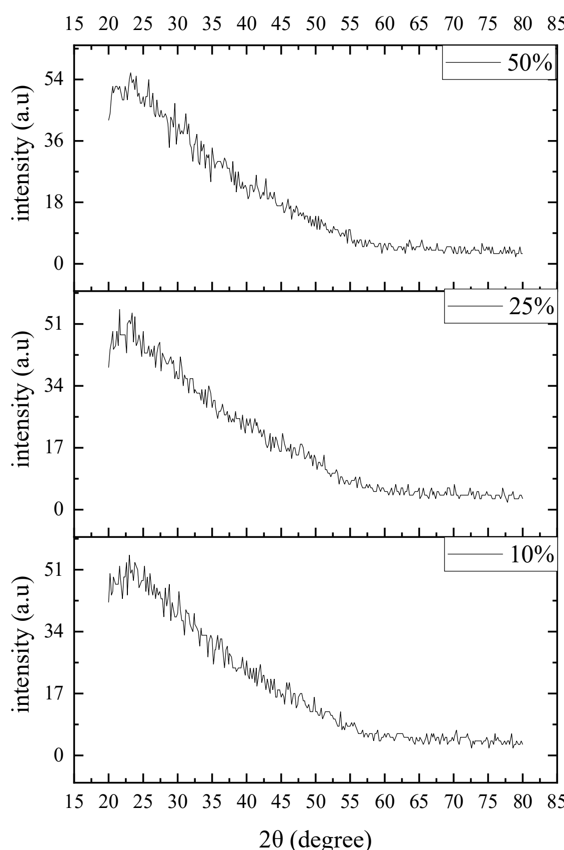

FIG. 1. XRD patterns of TiO_2 thin films.

3.2 Surface Morphology:

Representative roughness and 3D AFM images of the TiO_2 thin films deposited at different oxygen ratios are presented in Fig. 2 with an area of 12.1 µm×12.1µm. Table 2 shows height parameters and feature parameters after

applying a Gaussian filter (according to ISO-25178) [27-29]. The 3D view of AFM images shows the changes in the surface structure of these films, with heterogeneous peaks at their heights. Minor changes in the root-mean-square (RMS) height Sq values can be observed in Table 2. The films have low roughness due to the low deposition power, which was 550W. This agrees with Serio *et al.* [24], when they deposited TiO_2 thin films on unheated glass by DC magnetron sputtering at different oxygen ratios and power of 500 W, and produced films with a low roughness of around 6 nm. Fouda got ultra-smooth films with RMS of 0.5 nm, when he deposited TiO_2 thin films onto quartz by RF magnetron sputtering at $Ar:O_2$ ratio of 0.05 and 300W RF power [8]. The values of skewness Ssk and kurtosis Sku increase as the oxygen ratio increases. According to the values of Ssk and Sku, TiO_2 thin film with a thickness of 140 nm has more tapered peaks and long tails compared to the other deposited films. This agrees with the definitions of Ssk and Sku [28, 30]. Fig. 3 shows the corresponding distributions of the peak heights observed on the surfaces of the TiO_2 thin films. The vertical axis represents the number of peaks per unit area. The average grain size of the surface was about 16, 24, and 30 nm for deposited samples at oxygen ratios of 10%, 25%, and 50%, respectively. This indicates that the TiO_2 thin films have a nanostructure. An increase in the mean size of the grains was observed with an increase in the oxygen content. This change may be due to the change in the deposition rate [31].

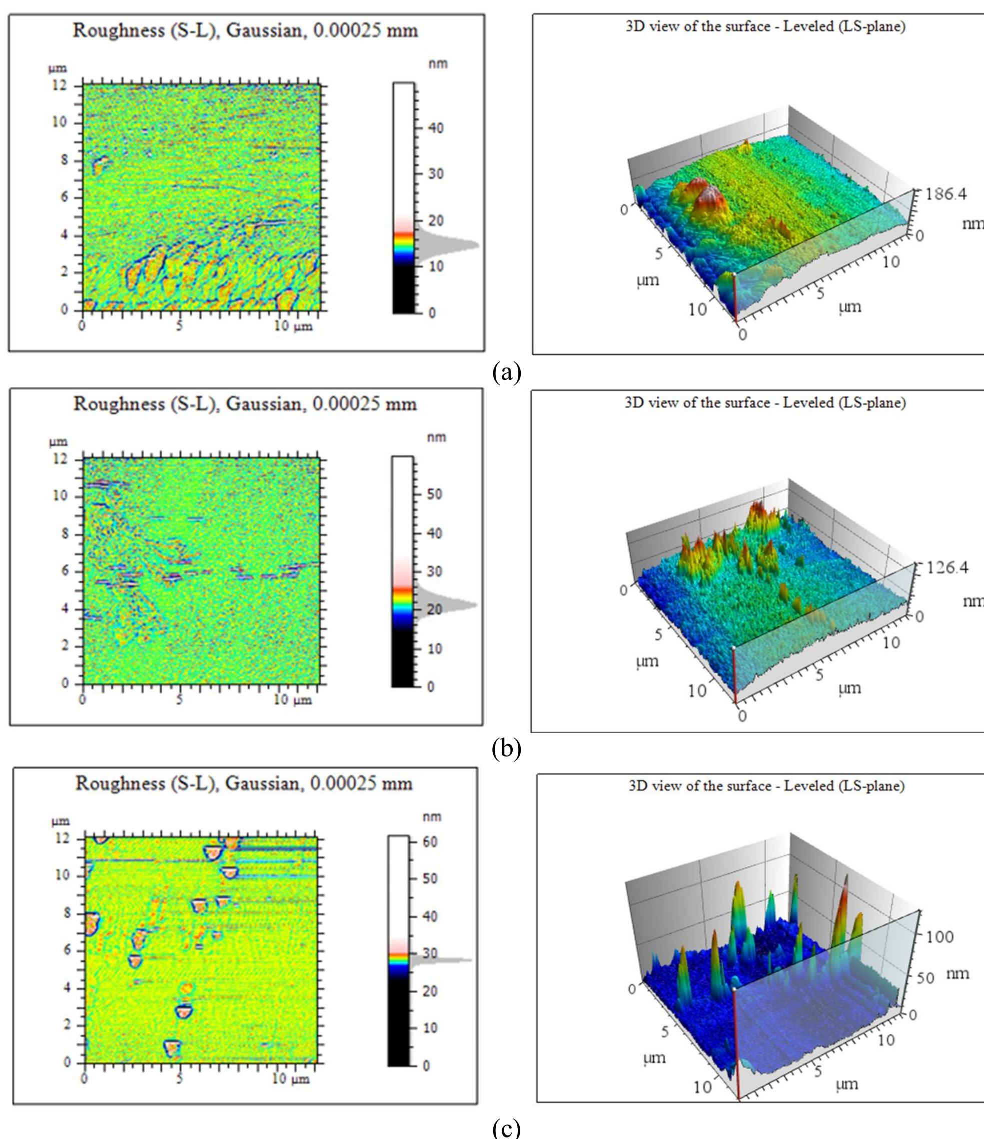

FIG. 2. Roughness (according Gaussian filter) and 3D AFM images of samples that deposited at (a) 10%, (b) 25%, and (c) 50% oxygen ratio.

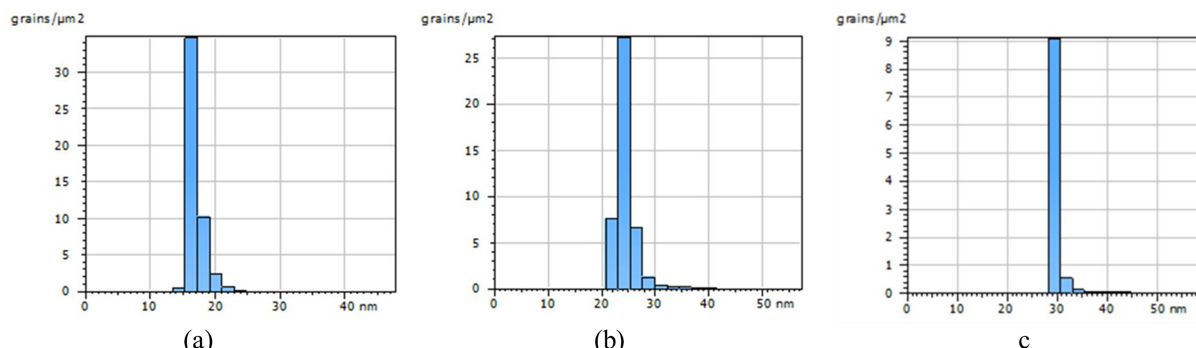

FIG. 3. Distributions of the peak heights per unit area of TiO_2 nanostructure thin films for thicknesses (a) 200 nm, (b) 184 nm and (c) 140 nm.

3.3 Optical Properties:

The transmittance spectra of TiO_2 thin films deposited at different oxygen ratios are studied. Fig. 4 shows the transmittance spectra of as deposited TiO_2 thin films as a function of wavelength in the range of 300-2000 nm. It is clear that the transmittance increases with the increase of both wavelength and oxygen content in the films. When the oxygen ratio is low, the transmittance of the films is low. This result agrees with previous literature [25, 26]. This may be due to nonstoichiometric film formation in material ratios [25]. When the oxygen ratio increases to 25% and 50%, then the oxygen becomes sufficient to fill the oxygen vacancies [32]. In addition, this reduces the loss of optical energy caused by free carrier absorption and photon scattering [33, 34]. Therefore, these two films are transparent with transmittances reaching 90% in the visible and near-infrared regions. It is observed from the spectra that the transmittance increases sharply at 400 nm. This region is called the fundamental absorption edge [19]. This indicates that the deposited films have a large band gap [35].

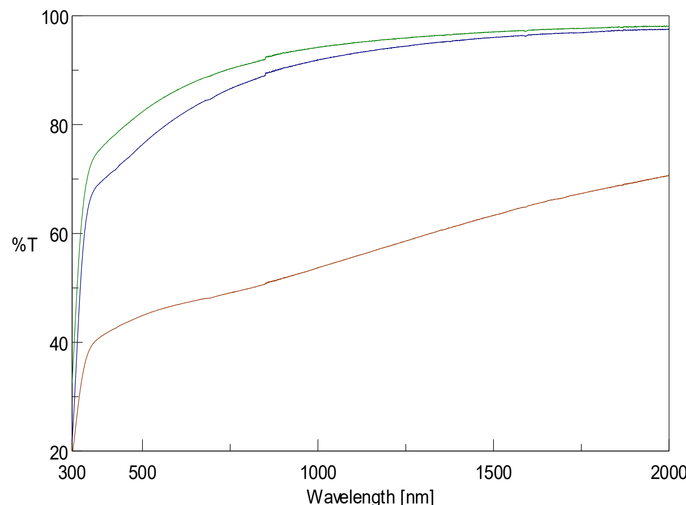

FIG. 4. The optical transmittance as a function of wavelength of TiO_2 thin films at different oxygen ratios.

An increase in transmittance leads to a decrease in the number of electronic transitions between valance and conduction bands. Horprathum *et al.* [36] reported that the transmittance of TiO_2 thin films deposited by DC magnetron sputtering has reached about 80% in the visible region at high oxygen partial pressure and DC power P = 100W. According to Nair *et al.* [37] and Mazur [38], the optical transmittance increased to more than 80%, when sputtering power was increased to P = 300W and 650W, respectively. It is also noticed that the transmittance decreased with increasing thickness of the films. This is attributed to the increase in deposition rate at low oxygen content, and then the oxygen molecules are less than sputtered titanium atoms. Therefore, there is a high possibility of depositing titanium atoms; here we have a high deposition rate and low oxidation of the target surface. As the oxygen

content increases, the target becomes completely oxidized, so both the deposition rate and thickness of the thin films decrease, which corresponds to the Refs. [23, 39]. The absorption coefficient α was calculated from the optical transmittance measurements, using the following equation [40]:

$$\alpha = \frac{1}{d}\log(\frac{1}{T}) \quad (2)$$

where d is the film thickness and T is the transmittance. The variation of absorption coefficient α of TiO_2 thin films was plotted as a function of photon energy hν in Fig. 5. A decrease in the values of the absorption coefficient was observed with the increase in the oxygen content in the films, due to the decrease in charge carriers. We found that the TiO_2 nanostructured thin films have both direct and indirect transmission mechanisms. The direct energy gap can be determined using the Tauc relation [15]:

$$(\alpha h\nu)^2 = A(h\nu - E_g) \quad (3)$$

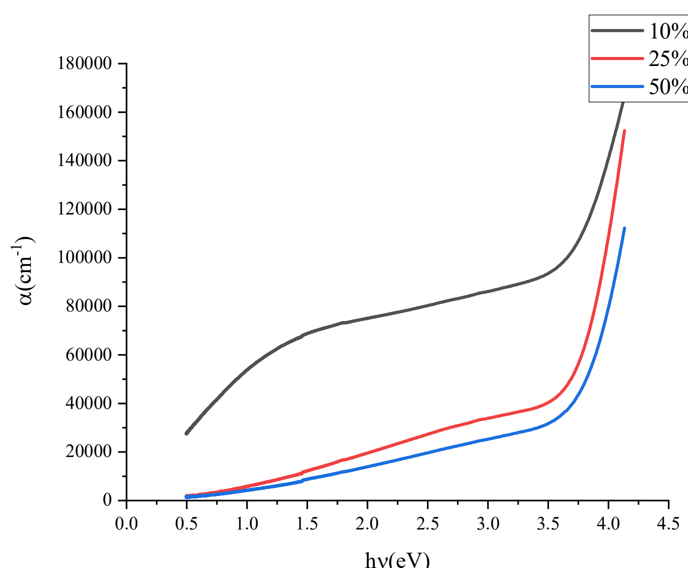

FIG. 5. Absorption coefficient as a function of photon energy.

The indirect energy gap was also determined using the Tauc relation [41]:

$$(\alpha h\nu)^{\frac{1}{2}} = A(h\nu - E_g) \quad (4)$$

where A is a constant, E_g is the energy band gap, and hν is the photon energy. The direct energy gap values were determined by the linear extrapolation of $(\alpha h\nu)^2$ in terms of $h\nu$., as shown in Fig. 6(a). Similarly, the indirect energy gap values were determined by the linear extrapolation of $(\alpha h\nu)^{\frac{1}{2}}$ in terms of $h\nu$., as shown in Fig. 6(b). Table 3 shows the calculated optical energy gap values of TiO_2 thin films. These resulting values are consistent with the results of Serpone *et al.* [42] and Odah *et al.* [43], when they deposited nanostructures of TiO_2 thin films. An increase in the energy gap of TiO_2 thin films was observed with the increase in oxygen ratio. The change in the structure of films is the decisive factor in the change in the energy gap. The increase in oxygen content reduces defects, thus reducing the number of charge carriers. Therefore, the number of sub-levels between valance and conduction bands decreases, so the transmittance and energy gap increase. This is in agreement with the literature [7, 23, 37, 44-46]. The energy gap of TiO_2 thin films deposited was larger than the energy gap for bulk materials, which indicates to formation of nanoparticles [47]. The difference in energy gap values between bulk and nanomaterials is due to the difference in atomic orbitals and bands. The nanomaterials have larger gaps, and they consist of more discrete energy levels. This is due to quantum confinement in the nanoparticles, which causes an increase in the energy gap. While bulk materials consist of several thousand atoms that contribute to the formation of highly overlapping orbitals, the energy gap becomes smaller [48, 49]. The Urbach energy shows the relation between the disorder of the structure and the energy gap [7]. The Urbach tail appears in weakly crystallized or amorphous materials [50].

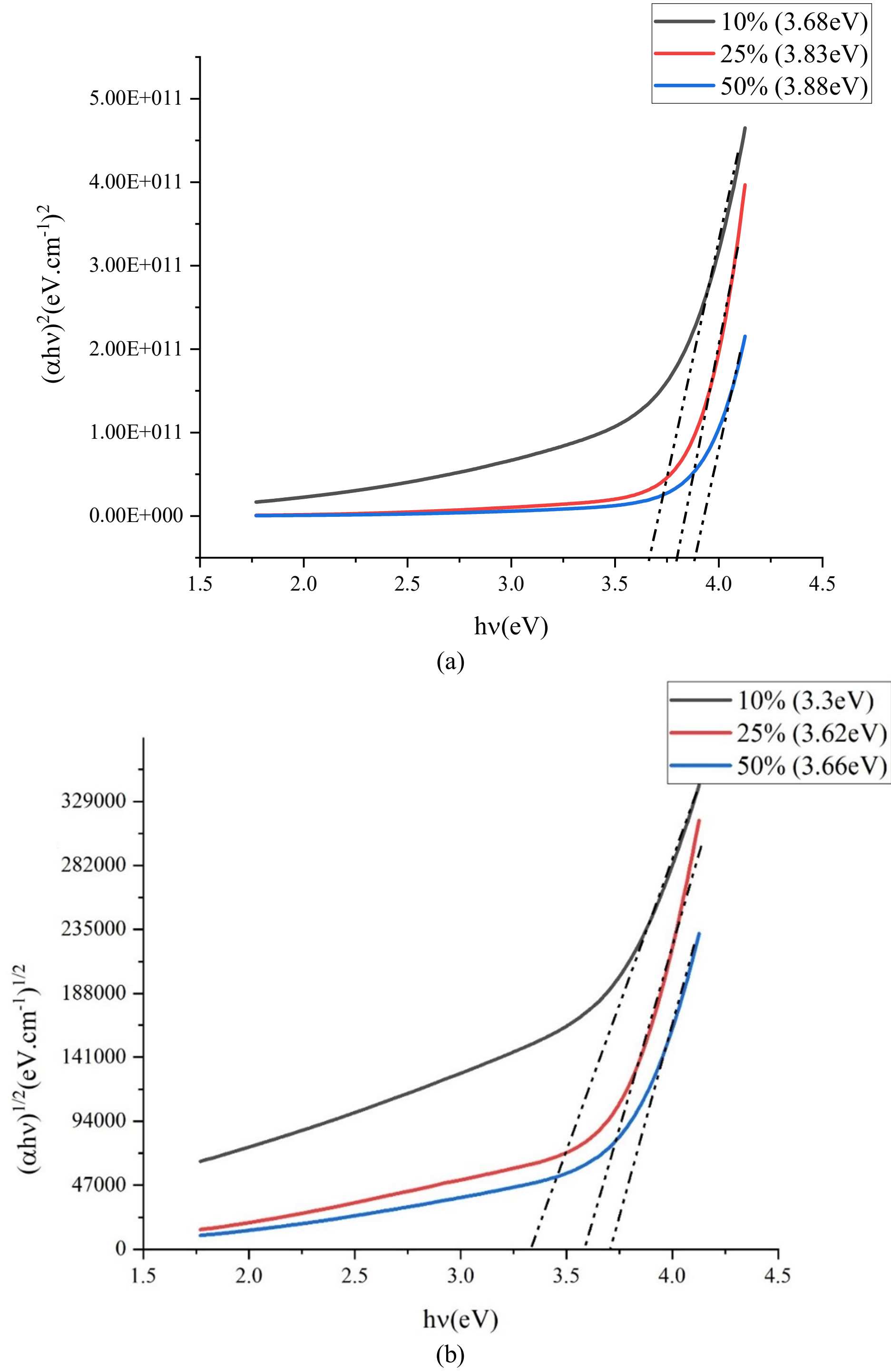

FIG. 6. (a) The optical allows direct energy gap, (b) the optical allows an indirect energy gap for TiO_2 thin films at different oxygen ratios.

TABLE 3. Values of optical band gaps and Urbach energy.

O_2 %	10	25	50
Direct band gap (eV)	3.68	3.83	3.88
Indirect band gap (eV)	3.3	3.62	3.66
Urbach energy E_u (eV)	0.848	0.332	0.311

The region in which the absorption coefficient increases exponentially is called the Urbach edge. The Urbach tail energy values were calculated in the low photon energy range, by applying the absorption equation for TiO_2 thin films [51]:

$$\alpha = \alpha_0 e^{\frac{h\nu}{E_u}} \quad (5)$$

where α_0 is a constant related to the type of material, E_u is the Urbach energy, and hν is the photon energy. Fig. 7 shows the curves of $\ln(\alpha)$ vs. hν to calculate Urbach energy. The values of E_u are calculated from the inverted tangent of the linear region of these curves. According to the calculated Urbach energy values presented in Table 3, an increase in E_u was observed with increasing thickness, in the inverse of band gap values. This indicated an increase in the localized energy levels in the energy gap. It is also noted from the values of E_u, that E_u decreases with the increase in oxygen ratio. This confirms the XRD results, which show amorphous phases. This is in agreement with Refs. [7, 50-54]. Extinction coefficient k and refractive index n are important optical constants in optical device design [46, 54]. The extinction coefficient k expresses light loss due to scattering and absorption in the thin films [50, 54]. The refractive index n determines the behavior of light in the material [5]. The refractive index is related to both film thickness and density [54, 55]. The extinction coefficient k and refractive index n values were found from the following relations [5]:

$$n = \left[\left(\frac{1+R}{1-R}\right)^2 - (k^2+1) \right]^{\frac{1}{2}} + \frac{1+R}{1-R} \quad (6)$$

$$k = \frac{\alpha\lambda}{4\pi} \quad (7)$$

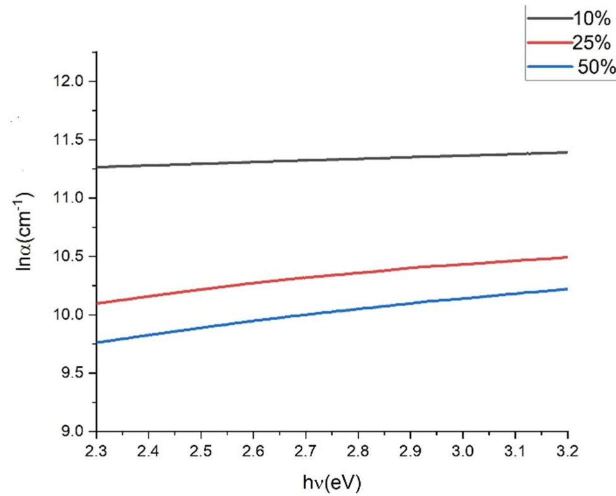

FIG. 7. A curve of lnα against the photon energy hν for TiO_2 thin films with different oxygen ratios.

The changes in the extinction coefficient k and refractive index n with the wavelength are shown in Figs. 8(a) and 8(b), respectively. It was noticed from Fig. 8(a) that the extinction coefficient k decreases with the increase in oxygen ratio. When the oxygen ratio increases, the optical transmittance increases, and the energy lost by scattering decreases. This agrees well with Refs. [37, 46]. It was also observed from the curves that the values of extinction coefficient k decrease with increasing wavelength for TiO_2 thin films deposited at 25% and 50% oxygen ratios. This means that there is a decrease in light loss occurs with an increase in wavelength. It was observed that the values of k of these two films are very close to zero in the visible range. This is consistent with the fact that these two films are transparent in this region. The values of extinction coefficient k increase sharply at a low wavelength (high photon energy region), this may be due to the electron transition from the valance band to the conduction band. This is compatible with the literature [50, 56]. As for the refractive index, it was observed from Fig. 8(b) that the highest value of refractive index n is related to the TiO_2 thin film deposited at 10% oxygen ratio, which indicates that this film is dense. The collisions of the deposition molecules decrease when the oxygen content is low, so the film has a high filling density [26]. The refractive index values decreased from 2.1 to 1.4 at λ = 500 nm when the oxygen ratio increased from 10% to 50%. This may be due to the decrease in the oxygen vacancies, which leads to a decrease in the concentrations of charge carriers. These refractive index values are in harmony with the results reported in the literature [46, 51].

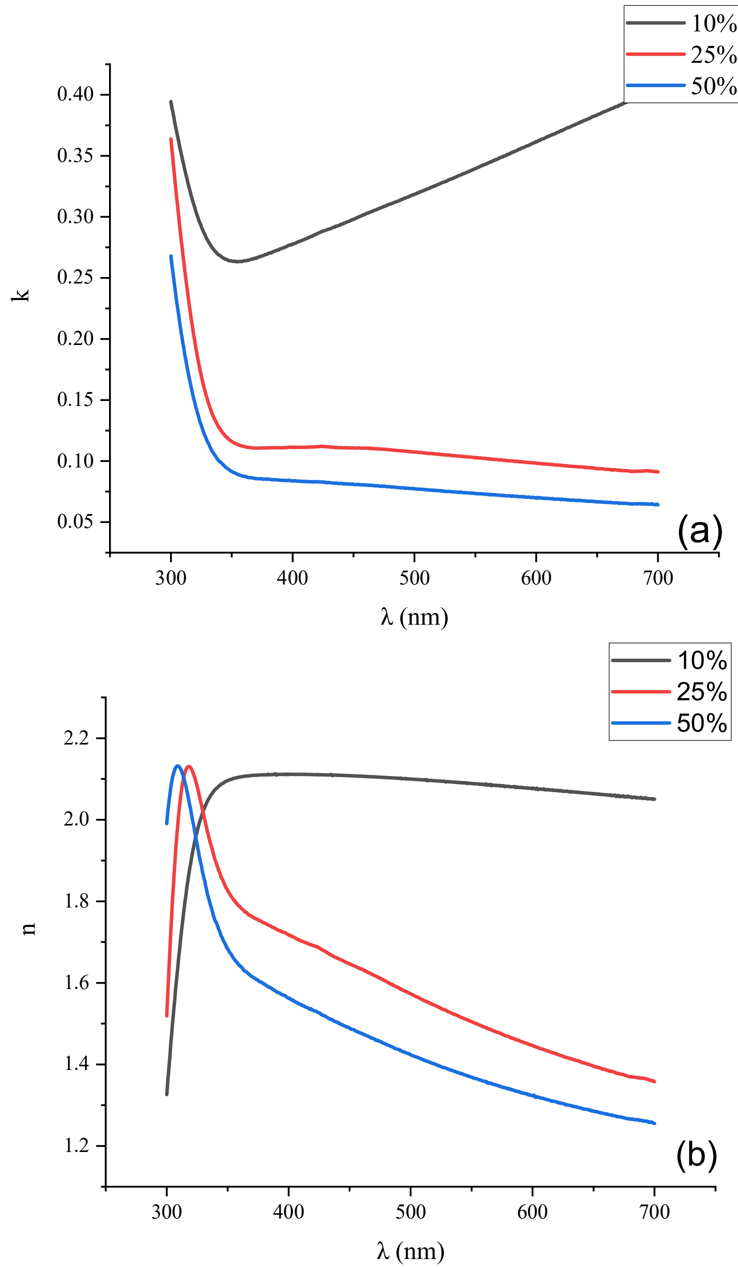

FIG. 8. (a) The extinction coefficient and (b) The refractive index of TiO_2 thin films deposited at different oxygen ratios.

The optical dielectric constant is defined as [46]:

$$\varepsilon = \varepsilon_r + i\,\varepsilon_i \quad (8)$$

The real part ε_r and the imaginary part ε_i of the dielectric constant are calculated from equation [55]:

$$\varepsilon_r = n^2 - k^2$$
$$\varepsilon_i = 2nk \quad (9)$$

It is noticed from plots in Figs. 9(a) and 9(b) that the values of both ε_r and ε_i decrease with the increase of oxygen ratio. From the curves in Figs. 9(a) and 9(b), it is observed that the values of ε_r are greater than the values of ε_i where n > k. This indicates that the amount of dissipated energy is less than the amount of energy stored in the deposited thin films. This is compatible with Refs. [7, 46, 50, 56]. The loss factor tanδ can be calculated by relation [57, 58]:

$$\tan\delta = \frac{\varepsilon_i}{\varepsilon_r} \quad (10)$$

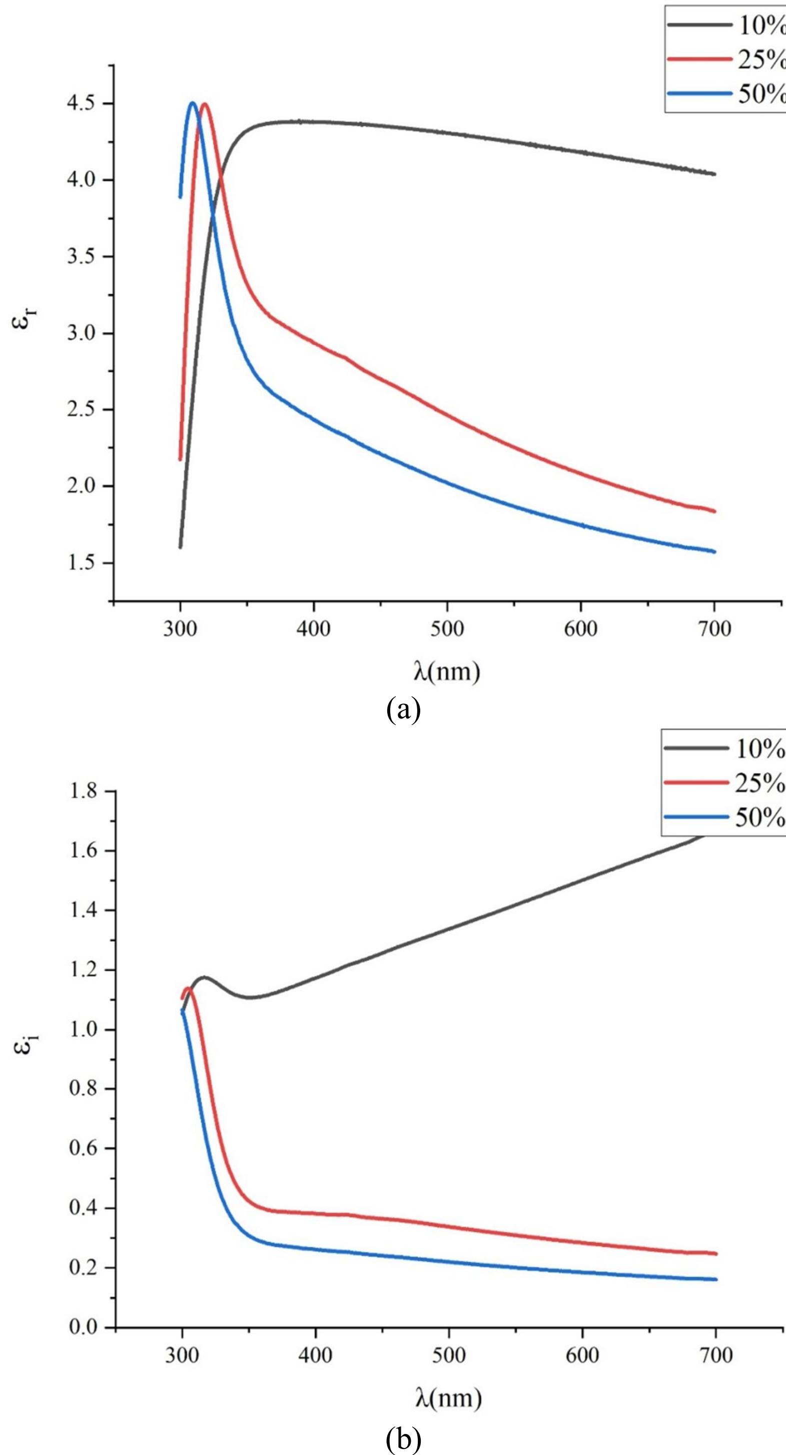

FIG. 9. (a) The real and (b) imaginary parts of the dielectric constant for TiO_2 thin films deposited at different oxygen ratios.

The loss factor values describe the dielectric behavior of TiO_2 thin films. The plots of the loss factor as a function of wavelength are shown in Fig. 10. It is observed from Fig. 10 that the loss factor decreases with increasing wavelength in the range of 300-350 nm. This indicates that, at high photon energies, electrical energy is lost in materials with large energy gaps [37, 46, 56, 59].

The optical conductivity σ_{opt} can be calculated by using [57]:

$$\sigma_{opt} = \frac{\alpha n c}{4\pi} \tag{11}$$

where α is the absorption coefficient, n is the refractive index, and c is the light velocity.

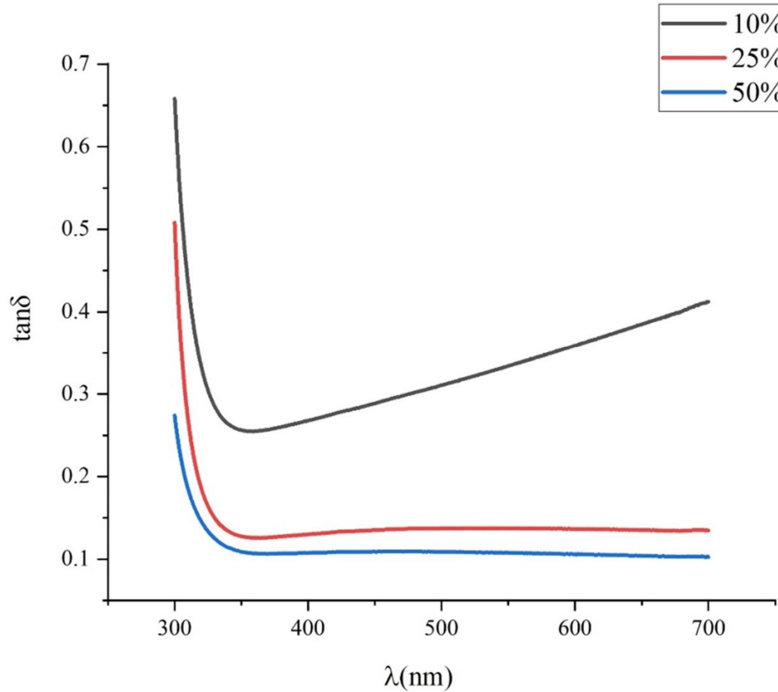

FIG. 10. The variations in loss factor with wavelength of TiO_2 thin films.

Fig. 11 shows the variation of σ_{opt} for TiO_2 thin films deposited at 10, 25, and 50%, as a function of photon energy. The optical conductivity σ_{opt} increased gradually with increases in the energy in the range of 1.7-3.5 eV. Then it increases rapidly in the range of wavelength corresponding to the optical energy gap (at high photon energies). This is due to the increase of the excited electrons as a result of the light beam falling on the semiconductor thin film, which causes an increase in absorption. Moreover, the optical conductivity decreases with an increase in oxygen ratio. It can be attributed to the decrease in oxygen vacancies. These results are in perfect agreement with the literature [37, 46, 54, 56, 57].

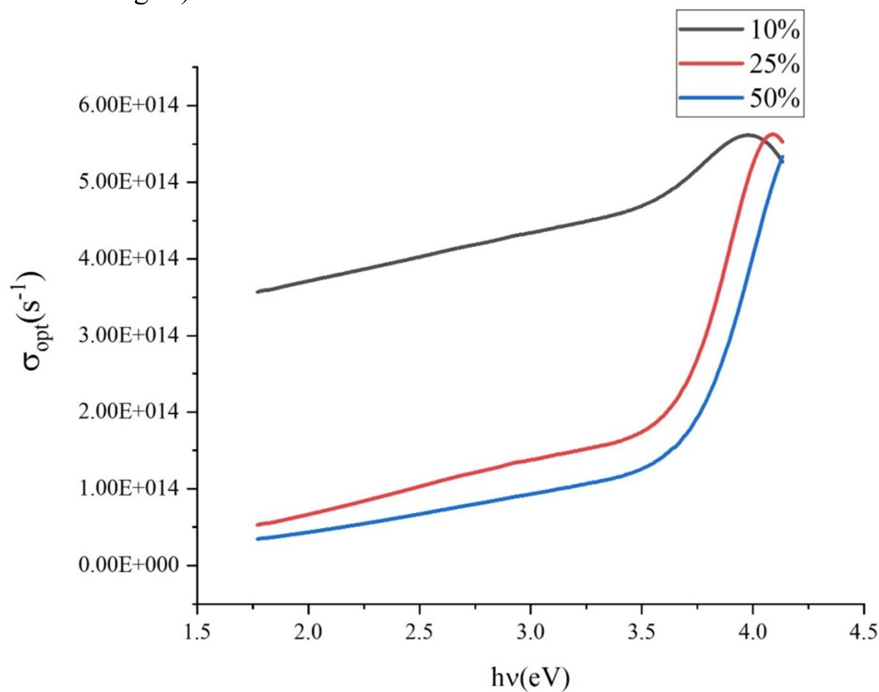

FIG. 11. Dependence of optical conductivity on photon energy of TiO_2 thin films.

3.4 Photoluminescence Study:

Using the fluorescence spectrometer, PL spectra of TiO_2 thin films were found at room temperature in the wavelength range of 200-900 nm. No fluorescence peaks were observed for the sample deposited at 10% O_2. The PL emission of TiO_2 samples deposited at 25% and 50% oxygen ratios occurs in ultra-violet and visible regions. The fluorescence peak intensity increases with increasing oxygen content in the thin films. Fig. 12 shows the PL spectra of TiO_2 thin film deposited at 25% oxygen ratio. An emission peak was observed at 3.3eV (376 nm), which can be ascribed to the excitons located at the surface defect levels [21]. Excitonic photofluorescence results from structural defects such as oxygen vacancies [37, 60, 61]. Other peaks were observed at 3.4eV and 3.2eV, which can be attributed to the band-band recombination and energy gap absorption, respectively. Baoshun Liu *et al.* [62] obtained emission of TiO_2 thin film in the UV-Vis range at room temperature, it was clearest at 3.4eV. As for TiO_2 thin film at 50% oxygen ratio, clear peaks were observed at 3.47eV (357 nm) for all excitation wavelengths in Fig. 13. The emissions are attributable to the recombination of photo-induced carriers.

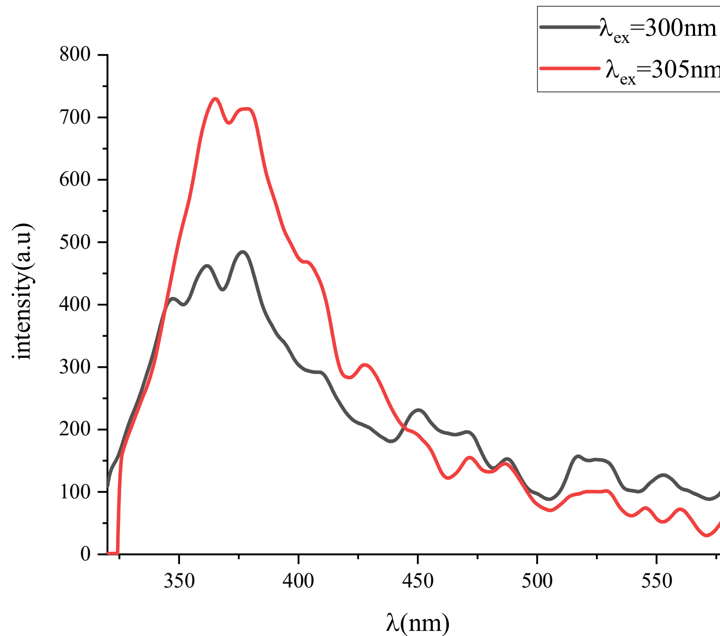

FIG. 12. PL spectra of TiO_2 thin films deposited at 25% O_2.

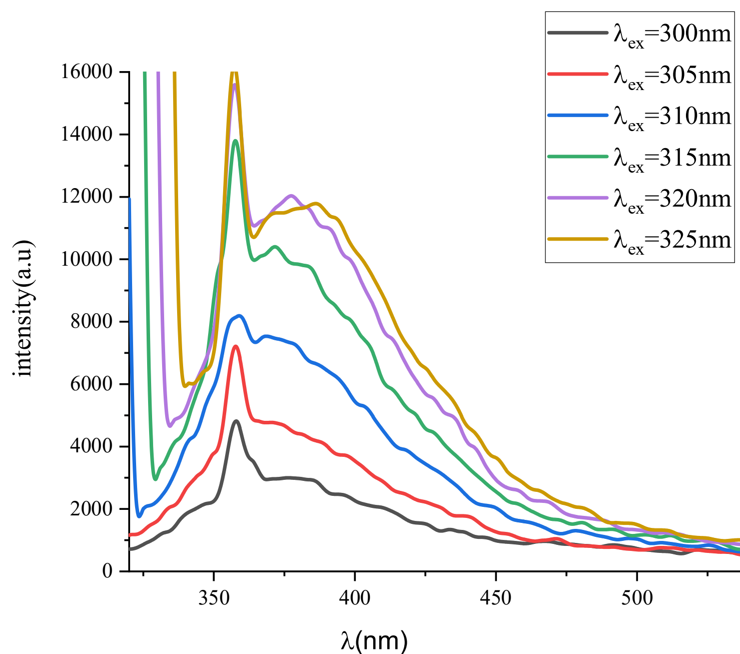

FIG. 13. PL spectra of TiO_2 thin film deposited at 50% O_2.

Table 4 shows the spectral values of the fluorescence of TiO_2 thin films deposited at 25% and 50% oxygen ratios. Since the full width at half maximum FWHM values is small, so PL emission in UV and visible regions suggests using these films in light emitters in the visible region [37, 63].

TABLE 4. The spectral values of the fluorescence of TiO_2 thin films deposited at 25% and 50% oxygen ratios.

λ_{ex} (nm)	Band start (nm)	Band end (nm)	λ_{PL} (nm)	FWHM	Int (cnt)	Fig.
300	320	580	376.7	74.7	480	12
305	324	540	365.2	67	730	
300	320	460	357.9	35.4	5750	
305	320	480	357.7	39.4	7150	
310	325	500	359	65	8000	13
315	328	520	357.6	54.7	13500	
320	334	520	357.7	39.9	15500	
325	340	540	357.2	59.8	15700	

3.5 Impedance Spectroscopy Study:

Fig. 14 shows the complex impedance spectra at different oxygen ratios of TiO_2 thin films. The complex impedance spectrum is useful in ensuring the homogeneity of the sample by studying the variations of the imaginary part X(ω) as a function of the real part R(ω). Complex impedance is given as:

$$Z(\omega) = R(\omega)+j\,X(\omega)$$

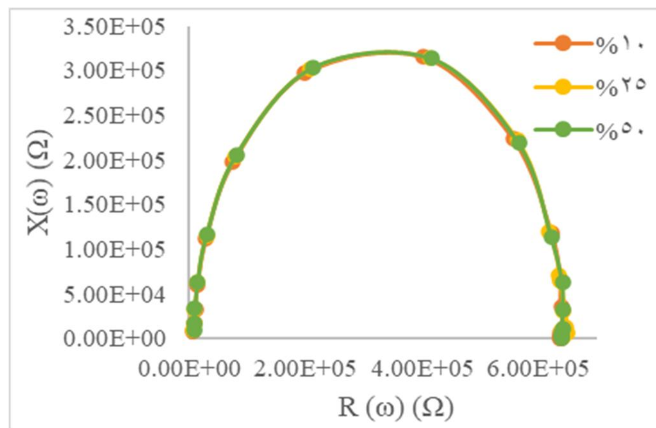

FIG. 14. Complex impedance plots for TiO_2 thin films deposited at different oxygen ratios.

The spectra show semi-regular semicircles, which correspond to the TiO_2 to Cole-Cole model [64]. This indicates here that the TiO_2 thin films have almost homogeneous grains and the equivalent circuit between each two grains of the film consists of a resistor connected in parallel with a capacitor [65, 66]. Table 5 shows the capacitance and resistance values, in addition to the real and imaginary values of complex impedance. No significant change in both diameter and maximum semicircle arcs was observed with changing oxygen content. This indicates that the change in the oxygen content did not affect the resistance. The capacitance values also demonstrate no significant changes, as there have been no alterations in the grain distributions within the films due to the absence of any heating procedures [65].

TABLE 5. The capacitance values, the real, and imaginary values of complex impedance.

O_2%	f(Hz)	$R(\omega)(\Omega)$	$X(\omega)(\Omega)$	$C_p(F)$
10	424	1.99E+5	2.97E+5	1.26E-9
25	424	2.08E+5	3.02E+5	1.24E-9
50	424	2.11E+5	3.04E+5	1.23E-9

4. Conclusion

Nanostructured titanium dioxide TiO_2 thin films were deposited on glass substrates by DC reactive magnetron sputtering at three different mixing ratios of $Ar:O_2$ without heating. The XRD patterns revealed that the TiO_2 thin films exhibited an amorphous phase.

AFM images showed a change in the surface morphology of the films as the oxygen content changed. From AFM data, it was found that the films have a nanostructure, which is consistent with the calculated band gap values. The low deposition power resulted in films with low roughness. The optical band gap values increased with the increase in oxygen content, while the behavior of the Urbach energy was the opposite. The extinction coefficient, the refractive index, and the loss factor decreased with the increasing wavelength. Values of the real part of the dielectric constant are greater than the values of the imaginary part. The optical conductivity increased with an increase in photon energy. The PL spectra of TiO_2 thin films showed that emissions occur in UV and visible regions for the films deposited at 25% and 50% oxygen ratios. Complex impedance measurements showed that the films have a nearly homogeneous structure and the resistance was not affected by changes in oxygen content.

References:

[1] Al-Oubidy, E.A. and Firas, J.K., Opt. Quant. Electron., 51 (1) (2019) 23.

[2] Guillén, C. and Herrero, J., Thin Solid Films, 636 (2017) 193.

[3] Shriwastava, S.K. and Singh, S., Int. J. Hybrid Inf. Technol., 9 (2) (2016) 267.

[4] Boyadzhiev, S., Georgieva, V. and Rassovska, M., J. Phys. Conf. Ser., 253 (1) (2010).

[5] Doubi, Y. et al., Appl. Phys. A-Mater, 127 (6) (2021) 1.

[6] Takeda, S. et al., Thin Solid Films, 392 (2) (2001) 338.

[7] Grilli, M.L. et al., Ceram. Int., 44 (10) (2018) 11582.

[8] Fouda, A.N., Appl. Phys. A-Mater., 126 (1) (2020) 1.

[9] Pansila, P., Witit-Anun, N. and Chaiyakun, S., Procedia Engineer., 32 (2012) 862.

[10] Ju, Y. et al., Energy Proced., 12 (2011) 450.

[11] Wang, Y.-H. et al., Catalysts, 10 (6) (2020) 598.

[12] Rao, M.C., Ravindranadh, K. and Shekhawat, M.S., AIP Conf. Proc., AIP Publishing LLC, 1728 (1) (2016).

[13] Kadri, L. et al., Coatings, 11 (5) (2021) 561.

[14] El Fanaoui, A. et al., J. Mater., 7 (3) (2016) 907.

[15] Balogun, S.W., Sanusi, Y.K. and Aina, A.O., Inter. J. Dev. Res., 8 (01) (2018) 18486.

[16] Shei, S.-C., Advances in Materials Science and Engineering, 2013 (2013).

[17] Kelly, P.J. and Arnell, R.D., Vacuum, 56 (3) (2000) 159.

[18] Al-Maliki, F.J. and Al-Oubidy, E.A., Physica B, 555 (2019) 18.

[19] Witit-anun, N. et al., Agric. Nat. Resour., 43 (5) (2009) 340.

[20] Cheng, X. et al., J. Cryst. Growth, 491 (2018) 120.

[21] Zhu, X. et al., Aip Adv., 7 (12) (2017) 125326.

[22] Musil, J., Heřman, D. and Šícha, J., J. Vac. Sci. Technol. A, 24 (3) (2006) 521.

[23] Triyana, K. and Nurwantoro, P., Research Gate, (2021).

[24] Sério, S. et al., Mater. Chem. Phys., 126 (1-2) (2011) 73.

[25] Chandra Sekhar, M. et al., J. Spectrosc., 2013 (2013).

[26] Shen, Y. et al., Opt. Laser Technol., 40 (3) (2008) 550.

[27] Introduction of surface roughness measurements, www.keyence.com.

[28] Siham, T., Abou Samra, R. and Imad, A., J. New Technol. Mater., 3 (1) (2013) 43.

[29] Blateyron, F., "The Areal Field Parameters", Characterisation of areal surface texture, (Springer, Berlin, Heidelberg, 2013) p. 15-43.

[30] Kumar, B.R. and Rao, T.S., Dig. J. Nanomater. Bios., 7 (4) (2012) 1881.

[31] Ghobadi, N. et al., J. Mater. Sci-Mater. El., 27 (3) (2016) 2800.

[32] Zhao, Y. et al., Appl. Surf. Sci., 210 (3-4) (2003) 353.

[33] Jeong, S.H. et al., J. Korean Phys. Soc., 41 (1) (2002) 67.

[34] Hossain, M.F., Pervez, M.S. and Nahid, M.A.I., Emerg. Mater. Res., 9 (1) (2020) 186.

[35] Ilican, S., Caglar, Y. and Caglar, M., J. Optoelectron. Adv. M., 10 (10) (2008) 2578.

[36] Horprathum, M. et al., Procedia Eng., 32 (2012) 676.

[37] Nair, P.B. et al., Prog. Nat. Sci-Mater., 24 (3) (2014) 218.

[38] Mazur, M., Opt. Mater., 69 (2017) 96.

[39] Poddar, S.K.M., Carbon-Sci. Tech., 8 (2) (2016) 1.

[40] Bedikyan, L., Zakhariev, S. and Zakharieva, M., J. Chem. Technol. Metall., 48 (6) (2013) 555.

[41] Sittishoktram, M., Ketsombun, E. and Jutarosaga, T., J. Phys. Conf. Ser., 901 (1) (2017).

[42] Serpone, N.I.C.K., Lawless, D.A.R.R.E.N. and Khairutdinov, R., J. Phys. Chem., 99 (45) (1995) 16646.

[43] Odah, J.F. et al., IOP Conf. Ser.: Mater. Sci. Eng., 454 (1) (2018).

[44] Kamble, S.S. and Radhakrishnan, J.K., Mater. Today: Proc., 45 (2021) 3915.

[45] Choudhury, B. and Choudhury, A., J. Lumin., 136 (2013) 339.

[46] Abd El-Moula, A.A., Raaif, M. and El-Hossary, F.M., Acta Phys. Pol. A, 137 (6) (2020).

[47] Pjević, D. et al., Thin Solid Films, 591 (2015) 224.

[48] Chen, L. and Park, C., Korean J. Chem. Eng., 34 (4) (2017) 1187.

[49] Ansari, M.Z. and Khare, N., Mater. Sci. Semicond. Process., 63 (2017) 220.

[50] Astinchap, B. and Laelabadi, K.G., J. Phys. Chem. Solids, 129 (2019) 217.

[51] Sta, I. et al., J. Sol-Gel Sci.Technol., 72 (2) (2014) 421.

[52] Mott, N. and Davis, E., "Electronic Process in Non-crystalline Materials", 2nd Ed., (Clarendon press, Oxford).

[53] Amato, A. et al., Sci. Rep., 10 (1) (2020) 1.

[54] Astinchap, B., Moradian, R. and Gholami, K., Mater. Sci. Semicond. Process., 63 (2017) 169.

[55] Abd El-Raheem, M.M. and Al-Baradi, A.M., Int. J. Phys. Sci., 8 (31) (2013) 1570.

[56] Akın, S. and Sönmezoğlu, S., Mater. Technol., 27 (5) (2012) 342.

[57] Abdel-Aziz, M.M. et al., Appl. Surf. Sci., 252 (23) (2006) 8163.

[58] Sönmezoğlu, S. and Sönmezoğlu, Ö.A., Mater. Sci. Eng. C, 31 (8) (2011) 1619.

[59] Assim, E.M., J. Alloys Compd., 465 (1-2) (2008) 1.

[60] Liqiang, J. et al., Sol. Energy Mater. Sol. Cells, 90 (12) (2006) 1773.

[61] Kavitha, A. et al., J. Mater. Sci.: Mater. Electron., 27 (10) (2016) 10427.

[62] Liu, B., Wen, L. and Zhao, X., Mater. Chem. Phys., 106 (2-3) (2007) 350.

[63] Guo, Z. et al., Adv. Mater., 33 (40) (2021) 2102246.

[64] Barsoukor, E. and Macdonald, J.R., "Impedance Spectroscopy (Theory, Experiment and Applications) ", 3rd Ed., (USA, 2018) p. 1-20.

[65] Jemaa, I.B., Chaabouni, F. and Ranguis, A., J Alloys Compd., 825 (2020) 153988.

[66] Quinonez, C., Vallejo, W. and Gordillo, G., Appl. Surf. Sci., 256 (13) (2010) 4065.